ACS NANO

www.acsnano.org

ARTICLE

Automated Gold Nanorod Spectral Morphology Analysis Pipeline

Samuel P. Gleason,* Jakob C. Dahl, Mahmoud Elzouka, Xingzhi Wang, Dana O. Byrne, Hannah Cho, Mumtaz Gababa, Ravi S. Prasher, Sean Lubner, Emory M. Chan, and A. Paul Alivisatos*

Cite This: *ACS Nano* 2024, 18, 34646−34655

Read Online

ACCESS | Metrics & More | Article Recommendations | Supporting Information

ABSTRACT: **The development of a colloidal synthesis procedure to produce nanomaterials with high shape and size purity is often a time-consuming, iterative process. This is often due to quantitative uncertainties in the required reaction conditions and the time, resources, and expertise intensive characterization methods required for quantitative determination of nanomaterial size and shape. Absorption spectroscopy is often the easiest method for colloidal nanomaterial characterization. However, due to the lack of a reliable method to extract nanoparticle shapes from absorption spectroscopy, it is generally treated as a more qualitative measure for metal nanoparticles. This work demonstrates a gold nanorod (AuNR) spectral morphology analysis tool, called AuNR-SMA, which is a fast and accurate method to extract quantitative structural information from colloidal AuNR absorption spectra. To demonstrate the practical utility of this model, we apply it to three distinct applications. First, we demonstrate this model's utility as an automated analysis tool in a high-throughput AuNR synthesis procedure by generating quantitative size information from optical spectra. Second, we use the predictions generated by this model to train a machine learning model to predict the resulting AuNR size distributions under specified reaction conditions. Third, we apply this model to spectra extracted from the literature where no size distributions are reported and impute unreported quantitative information on AuNR synthesis. This approach can potentially be extended to any other nanocrystal system where absorption spectra are size dependent, and accurate numerical simulation of absorption spectra is possible. In addition, this pipeline could be integrated into automated synthesis apparatuses to provide interpretable data from simple measurements, help explore the synthesis science of nanoparticles in a rational manner, or facilitate closed-loop workflows.**

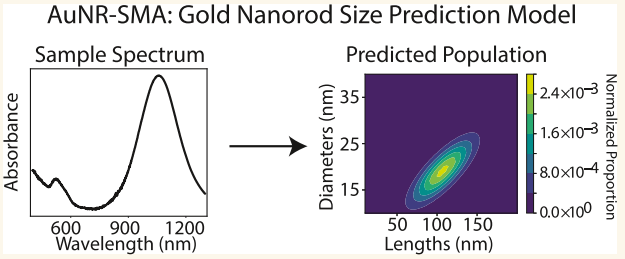

KEYWORDS: *machine learning, automated analysis, Au, nanorods, nanoparticle synthesis, high-throughput*

INTRODUCTION

Gold nanorods (AuNRs) have drawn significant research efforts due to their applications in cancer cell imaging and treatment, particularly in the development of photothermal therapies,[1−9] surface-enhanced raman spectroscopy,[9−12] and photovoltaic devices.[9,13,14] These applications rely on the localized surface plasmon resonance (LSPR) of AuNRs, which is highly dependent on the shapes and sizes of these nanoparticles.[9,15−17] The LSPR of AuNRs is tuned primarily by changing the ratio of length to width, or aspect ratio (AR), of the nanorods.[15−17] Applications of AuNRs thus require the synthesis of these particles with a high shape yield and narrow size distributions. However, it remains a challenge to quantitatively understand the impact of AuNR synthesis parameters on the resulting AuNRs.[18] Quantitatively determining the size and shape distributions of AuNRs requires direct measurement using electron microscopy, which is a time, resource, and knowledge intensive task,[19,20] limiting the amount of data that can be gathered to train models to predict synthesis outcomes.[21] Although progress has been made automating the size measurement of metal nanoparticles from transmission electron microscopy (TEM) images,[19,20,22] the hardware required for the automation of TEM image collection is not widely available.[23] Therefore, we have built an automated analysis model that can extract population level size information from absorption spectroscopy as a tool for more scalable analysis of AuNRs.

Recent work has found success predicting the sizes of individual AuNRs from single particle absorption spectra[24] and has found limited success at matching individual simulated

Received: July 19, 2024
Revised: November 27, 2024
Accepted: December 5, 2024
Published: December 13, 2024

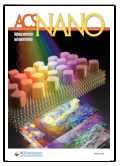

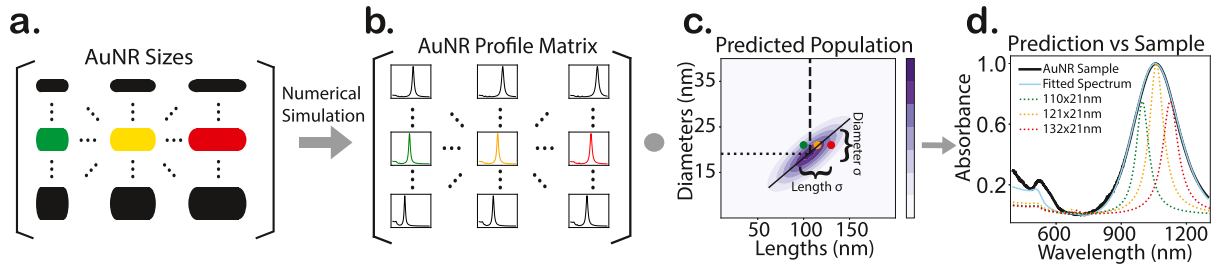

Figure 1. Outline of the SMA showing (a) how a 2D matrix of AuNR sizes was numerically simulated and (b) entered into a matrix with identical dimensions to (a). The fitted population distribution is projected onto a 2D matrix (c) and combined with (b) via a dot product to produce the simulated mixture spectrum (d). This step is repeated with different population distributions (c) until the simulated mixture spectrum (d) achieves the best possible fit to the inputted experimental spectrum. More details on this process can be found in the Supporting Information, section "Spectral Morphology Analysis Outline".

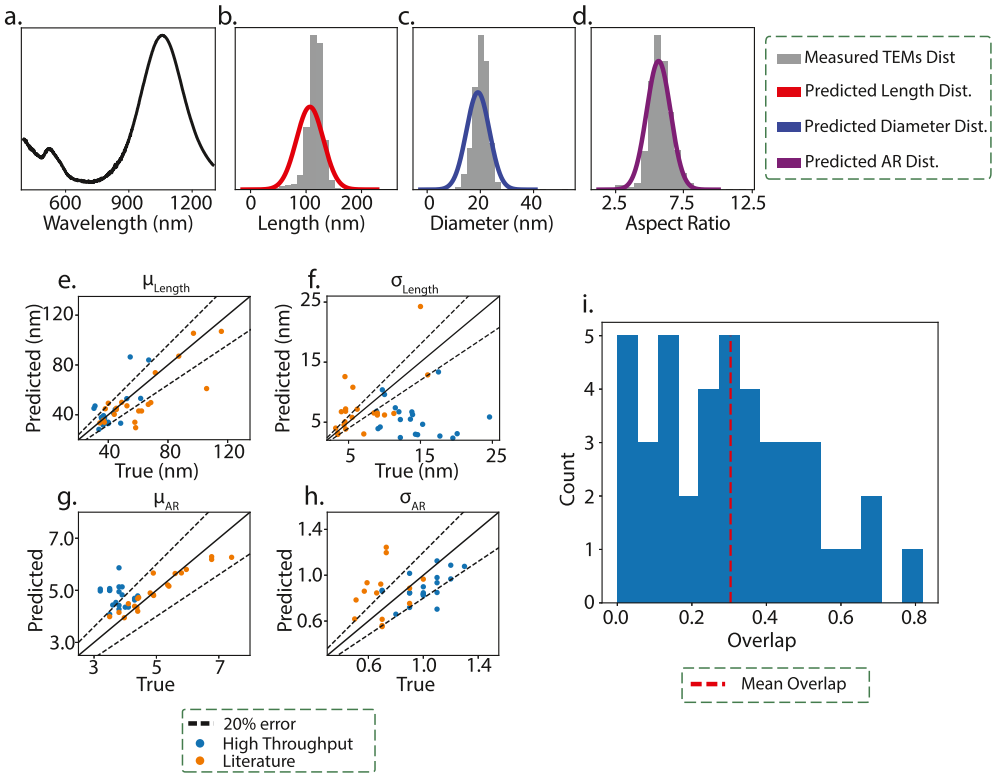

Figure 2. Accuracy of the SMA. (a–d) Sample AuNR spectrum (a) and an example of the model output in 1D (b–d). The predicted length distribution (b) is shown in red, the predicted diameter distribution (c) is shown in blue, and the predicted AR distribution (d) is shown in purple. The predicted distributions are plotted over histograms produced by manually measuring AuNRs taken from TEM images. For our 41 validation samples, the accuracy of their size parameters is shown in (e–h). The predictions are colored by whether they came from our high-throughput samples (blue) or literature spectra (orange). μ_{Length} (e) and σ_{Length} (f) are the length mean and standard deviation, respectively. μ_{AR} (g) and σ_{AR} (h) are the AR mean and standard deviation, respectively. (i) Histogram of the overlap between the predicted 2D distribution in length and diameter space and the true distribution, with the mean overlap indicated with a dashed red line.

single particle absorption spectra to samples with very narrow size distributions.[25] However, it remains a challenge to provide accurate population level size information for experimental spectra from a sample with a wide size distribution of AuNRs or where spherical AuNPs (AuNS) are also present. An analytical method that can determine AuNR size and shape distributions from absorption spectra and overcome issues related to impure samples[26,27] creates opportunities for developing interpretable models of AuNR synthesis.

Here, we overcome these challenges by focusing on the regions of the spectrum where degeneracies from AuNS and left over unreacted growth solution are minimized and selecting spectra according to a series of internal uncertainty metrics. We also enable the prediction of population-level statistics by fitting a 2D Gaussian ensemble of simulated AuNR spectra directly to the measured spectrum. This is carried out using an optimization model that minimizes the difference between an ensemble simulated spectrum and the experimental spectrum. This approach provides much more information on the AuNR sample than existing techniques, which focus on matching single particle simulated spectra to an experimental spectrum.

We showcase the utility of our automated spectral AuNR morphology analysis in three applications:

1. automating the analysis of one-pot seedless high-throughput AuNR synthesis,

https://doi.org/10.1021/acsnano.4c09753
ACS Nano 2024, 18, 34646–34655

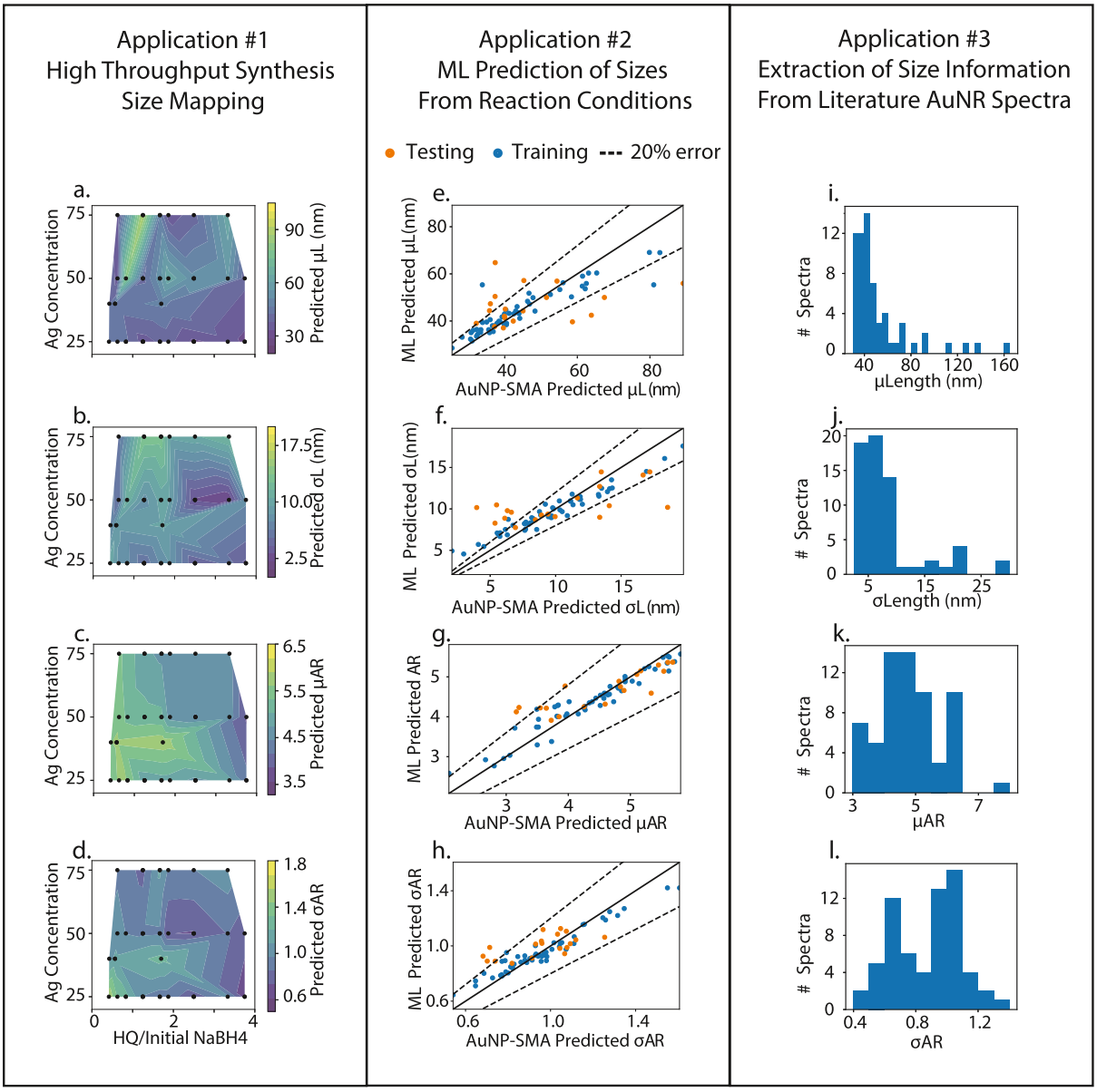

Figure 3. Application 1—2D representations showing how changing synthesis condition impacts the produced length mean (a), length standard deviation (b), AR mean (c), and AR standard deviation (d), generated using AuNR-SMA. The contour plots show how each of the four size parameters changes with the ratio of hydroquinone to initial $NaBH_4$ (*x*-axis) and the $AgNO_3$ concentration (*y*-axis). The black dots show where experiments have been conducted and predicted. Application 2—accuracy of the ML model trained to predict synthesized size distributions from reaction condition. This model is trained on the high-throughput experiments from Application 1 labeled by AuNR-SMA and augmented by the labeled high-throughput synthesis data used to validate AuNR-SMA. The model's accuracy on length mean (e), length standard deviation (f), mean AR (g), and AR standard deviation (h) are shown. Training accuracy is shown in blue while accuracy on test data is shown in orange. Application 3—distributions of size parameters from the 64 unlabeled literature spectra predicted in this work. Histograms of length means (i), length standard deviations (j), mean aspect ratios (k), and AR standard deviations (l) are shown.

2. training machine learning models to predict AuNR synthesis outcomes,
3. imputing quantitative synthesis data from literature spectra for which population level size data were not reported.

The first two applications comprise a highly active field of research, and AuNP synthesis has already been developed to include prediction of absorption spectrum from synthesis condition, and to rationally design conditions for a specified spectrum.[28−31] However, these procedures focus on relating the conditions to the resulting spectrum[28−30] or on AuNS synthesis and analysis.[31] This limits the abilities of these procedures to produce fundamental synthesis knowledge about how synthesis conditions lead to changes in the AuNP morphology, particularly under previously unexplored reaction conditions. More broadly, there is very limited quantitative information regarding how the AuNR synthesis conditions change the resulting AuNR sizes. In recent years, a few studies[18,28] have attempted to fill in this gap, but these have focused on the seed-mediated synthesis method for AuNRs. Therefore, we focus on the one pot, or seedless,[32] synthesis procedure, and combine the AuNR spectral analysis method we developed with liquid handling synthesis and characterization robots to build an automated synthesis and analysis

https://doi.org/10.1021/acsnano.4c09753
ACS Nano 2024, 18, 34646−34655

pipeline. We then utilize this pipeline to build a quantitative understanding of the seedless AuNR synthesis procedure and train machine learning models capable of predicting sizes and aspect ratios from initial concentrations of reagents. Using this model, we demonstrate the rich quantitative information that can be extracted from simple measurements and how this information can be applied to nanomaterials discovery.

RESULTS AND DISCUSSION

Automated AuNR Size Distribution Analysis. UV/vis/NIR absorption spectroscopy was selected as the analytical method for size distribution inference due to the ease of high-throughput characterization and the ability of absorption spectroscopy to simultaneously measure the absorption of every particle in the colloid. Additionally, absorption spectroscopy can be used without sample purification, which can significantly alter the sample's size distribution. Our spectral morphology analysis (SMA) model uses numerically simulated absorption spectra of single AuNRs to determine the length, diameter, and AR distributions of simulated AuNRs that most accurately reproduce the experimental spectrum. As such, this model can provide not only the mean lengths and aspect ratios of the sample but also ensemble level information. An outline of this model is shown in Figure 1.

The predictions of this model were validated by TEM analysis of 20 samples from a high-throughput synthesis experiment and 21 spectra extracted from the literature. Using AutoDetect-mNP,[20] we determined the size and shape distributions of AuNRs in each sample and compared them to the predictions generated from our model. The predictions of the literature spectra were compared to the size distributions reported in the paper. The accuracy of the predictions on our 41 validation spectra is shown in Figure 2.

Figure 2 shows an example set of outputs provided by this model and their validation against known measurements in 1D. Figure 2a–d shows a sample AuNR spectrum (a) and the predicted length (b), diameter (c), and AR (d) distributions plotted over histograms produced by manually measuring AuNRs taken from TEM images. The model outputs each of these 1D predictions as well as the 2D prediction in length and diameter space, as shown in Figure 1c. Using the size parameters produced by the model, the mean and standard deviation of lengths, diameters, and aspect ratios, we can determine the accuracy of this model by comparing to measured TEM images taken in this work or presented in the literature. Figure 2e–h shows these comparisons for length mean (e), length standard deviation (f), AR mean (g), and AR standard deviation (h). In general, the length means and AR standard deviations are quite accurate, showing very few samples outside of a 20% error line in either direction. The mean AR is highly accurate for the samples extracted from the literature, while showing a characteristic overestimation in our high-throughput synthesis samples. This can be attributed to changes in the tip geometry of the AuNRs caused by the synthesis developed by ref 33. Errors in length standard deviation can be attributed to the inherent difficulty in determining the ground truth of this parameter and the relatively low impact this parameter has on the overall appearance of the spectrum. More details can be found in the Supporting Information, section "Spectral Morphology Analysis Details".

As the distributions shown in Figure 2b–d are challenging to use as a model accuracy metric over an ensemble validation set, in this work, we express the accuracy as a comparison between the predicted 2D distribution of lengths and diameters and the measured distribution. We do this by calculating an overlap coefficient[34] between the predicted size distribution and the true distribution in length and diameter space (Figure S1). In the case of our high-throughput samples, where manual TEM measurements are available, the true distribution was projected onto a normal distribution to ensure accurate comparison with literature distributions, where only means and standard deviations are reported (Figure S2). For literature spectra, where the individually measured TEM particles are not available, the overlap was determined by calculating a distribution based on the reported AuNR means and standard deviations for length and diameter. Using this validation, this model has been shown to produce a predicted distribution which has a high degree of overlap. The average overlap across all the validation spectra is shown to be around 0.3 in Figure 2, showing that on average, this model is able to reasonably reproduce the population distribution of AuNRs present in the colloid (Figure S3).

Application 1—High-Throughput Synthesis Size Mapping. By systematically varying concentrations of $AgNO_3$, hydroquinone, initial $NaBH_4$, and total $NaBH_4$ (see Methods section-High-Throughput Synthesis) and utilizing our automated SMA model on the spectra of the resulting samples, we were able to determine trends in sizes and size distributions of the AuNRs. This high-throughput synthesis reaction produced 48 samples where rods were successfully synthesized. Of these 48 samples, six spectra could not be processed by our SMA due to high prediction uncertainty or a longitudinal peak at too high energy (Figure 4). Using the successfully fit samples, a synthesis map of the size parameters predicted from their absorption spectra, labeled by their reaction conditions, is shown in Figure 3a–d. The *x*-axis shows the ratio of hydroquinone to the first addition of $NaBH_4$, which was chosen due to the combination of these two conditions controlling the growth kinetics, which has been shown to be responsible for changing morphology in AuNR synthesis.[35] Additionally, interactions with the weak and strong reducing agents have also been shown to impact the sizes and yield of AuNRs.[18] $AgNO_3$ concentration was visualized on the *y*-axis due to myriad observations that $AgNO_3$ concentration is essential to controlling AuNR morphology.[18,36,37]

The predicted lengths show that at low $AgNO_3$ concentration, the maximum length produced with any combination of hydroquinone and $NaBH_4$ produces AuNR lengths from 30 to 50 nm. However, at higher concentrations of $AgNO_3$, lengths of 70–90 nm can be produced for specific hydroquinone and $NaBH_4$ ratios. As these resulting sizes are much less common for this synthesis procedure, one may be inclined to attribute this less common result to an error in the SMA. However, one of the two sets of conditions resulting in longer AuNRs contains two samples with the same ratio of reaction conditions, and those produced mean length predictions that were less than 10 nm apart, making it unlikely that a simple large error in the model is responsible for this result. Overall, we demonstrate that our model can be integrated into high-throughput experiments as an automated size distribution prediction tool, generating quantitative data on the fly. This allows for rapid detailed analysis and enables the possibility of closed loop workflows for the robotic AuNR synthesis.

Application 2—ML Prediction of Sizes from Reaction Conditions. Besides enabling a more quantitative under-

https://doi.org/10.1021/acsnano.4c09753
ACS Nano 2024, 18, 34646–34655

standing of AuNR synthesis, the ability to predict synthesis outcomes enhances synthetic exploration and optimization. By combining our synthesis and analysis pipeline with machine learning, we used reaction conditions to predict the resulting AuNR size distributions. Specifically, averages and standard deviations of the lengths and aspect ratios are predicted. We use a data set containing 73 samples, where reaction conditions were labeled by their resulting AuNR sizes. This data set was generated by augmenting the AuNR-SMA predictions from Application 1 with the labeled high-throughput synthesis data used to validate AuNR-SMA. We use the following algorithms, as implemented in scikit-learn,[38] to attempt to predict the output parameters from synthetic inputs: Elastic Net, Bayesian Ridge Regression, Kernel Ridge Regression, Support Vector Regression, Random Forest Regression, and Gradient Boosting Regression. Generally, random forest regression models outperformed k-nearest neighbor, support vector regression, kernel ridge regression, Bayesian Ridge regression, and elastic nets for most of this data set. Gradient boosting regression delivered similar results, though support vector regression performed better for predicting lengths and k-nearest neighbor models performed best for AR standard deviations (see Table S2). The models were reasonably well predictive for AR and standard deviations of aspect ratios, with test R^2 values of around 0.7 and ∼10% errors (Figure 3e−h). While length and length standard deviations were less well predicted, error ranges were similar to those of AuNR-SMA. Previous work using machine learning has shown the ability to predict spectral alignment of AuNRs in seeded growth synthesis.[28,29] We show here that it is possible to integrate the information gained from SMA with machine learning methods to directly predict the size and aspect ratios of AuNRs from their synthesis conditions in a one-pot, seedless growth procedure. In principle, this analysis routine could also be used in tandem with kinetic models to produce scientific machine learning models of particle growth.[39]

Application 3—Extraction of Size Information from Literature AuNR Spectra. In addition to this model's utility as an automated analysis tool for AuNR synthesis and our ability to generate predictions of AuNR morphology produced from reaction conditions, we also turn this model to the AuNR synthesis literature to impute size information from published spectra without direct size measurements. Our extraction produced 64 unlabeled literature spectra that were successfully fit by our model (Figure 3i−l). The most common aspect ratios reported in the literature were observed between 4 and 5, with a non-negligible spread higher into ARs of 5−6, although very few are seen greater than 7. Similarly, AuNR lengths of 30−70 nm are far more commonly seen in the literature than longer lengths, although rods greater than 100 nm have been successfully synthesized. Looking in detail at three synthetically interesting outliers that are predicted to have lengths >100 nm and where we found TEM images of similar synthesis outcomes in the same report,[33,40,41] the first comes from a publication reporting syntheses that result in rods with length >100 nm,[33] the second most likely has a length of roughly 90 nm,[42] and the third has TEM images showing rods with roughly 50 nm length.[40] A further detailed comparison and discussion of potential external factors that can induce errors in predictions can be found in the Supporting Information. Overall, we demonstrate that our model can be used to impute missing size and size distribution information from previous literature reports, contributing to a richer data ecosystem, allowing more in-depth analysis, and enabling machine learning based on previous literature results.

OUTLOOK

The above results have demonstrated the effectiveness of physics-based models to quantitatively predict the morphology of AuNRs in a colloidal sample from their absorption spectrum. It should be noted that this architecture is optimized for predicting AuNR samples when the colloid contains either pure AuNRs or mixtures of AuNRs and AuNS, where the AuNS are present in a small enough fraction that the longitudinal peak intensity is higher than that in the transverse region. If the fraction of AuNS is higher than this, or if other shapes of AuNPs are present in non trivial amounts, i.e., cubes, triangles, or pyramids, this architecture may struggle to accurately predict the AuNR sizes present in the colloid. This architecture may be extended to other colloidal nanoparticle samples provided the basic principles of this approach are met. First, the optical spectral parameters must change in response to the nanoparticle size/shape. This is true in many nanoparticle systems, particularly those with strong plasmonic excitation in the vis/NIR regions. These include other types of gold nanoparticles, including cubes[42] and triangles.[43] Beyond gold nanoparticles, this size/shape dependence on optical properties is seen in other noble metal nanoparticles, namely, silver[44] and copper[45] nanostructures, as well as quantum dots[46] and perovskite nanoparticles.[21] It must also be true that simulation procedures are or can be developed to be accurate enough to account for these changes and match the corresponding experimental spectra. Another practical experimental consideration is that if other unpredictable experimental factors change the spectrum, these must be separable from the spectrum or accounted for by fitting only a specific part of the spectrum, as was carried out in this work. For the full high-throughput synthesis and analysis pipeline presented here to be extendable, the above criteria must be met, and the nanoparticle size parameters must be tunable via the synthetic conditions.

CONCLUSIONS

In this work, we have developed AuNR-SMA, a physics-based automated SMA tool for colloidal AuNR samples. This model is able to predict the AuNR sample's length and AR mean and standard deviation with a high degree of accuracy, producing population level information on the produced AuNR sample from its absorption spectrum. We validated this model by comparing its predictions to measured AuNR size distributions extracted from TEM images and spectra labeled with size distributions extracted from the literature. We show this model's wide range of applications by utilizing it as an automated analysis tool in high-throughput AuNR synthesis, generating training data for rational synthetic design machine learning models, and as a literature mining tool to increase the volume of quantitative knowledge available on AuNR synthesis. Through these applications, we elucidate quantitative information about seedless AuNR synthesis using hydroquinone and the relationships between the reaction conditions and the size outcomes. In principle, this approach can be extended to any other nanocrystal system where the absorption spectra are size dependent, and accurate numerical simulation of the absorption spectra is possible.

https://doi.org/10.1021/acsnano.4c09753
ACS Nano 2024, 18, 34646−34655

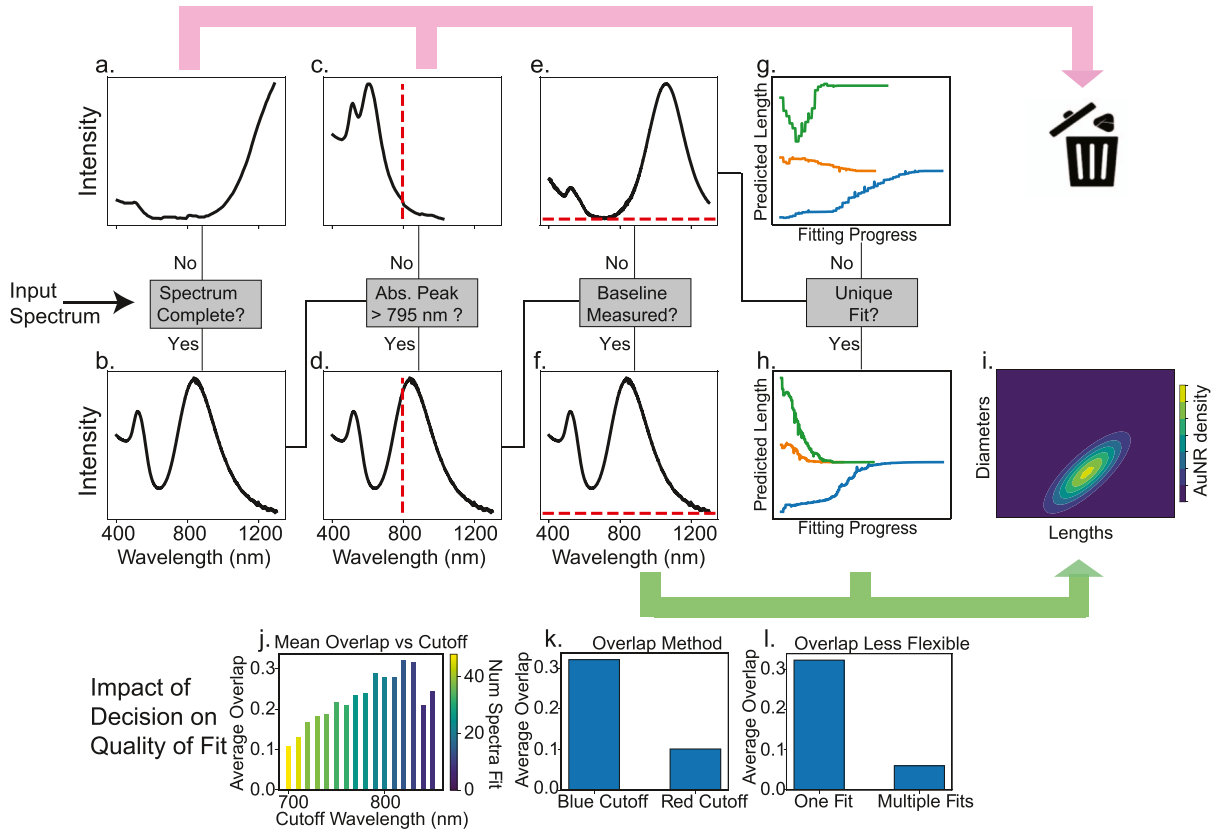

Figure 4. Steps the overall SMA uses to determine how, or if, an input spectrum is fit and whether the results of that fit are expected to be accurate. Briefly, the model first determines whether the input spectrum is complete (a,b) discarding incomplete spectra. The model then determines if the longitudinal peak is before or after 795 nm (c,d) discarding spectra with peak wavelengths shorter than 795 nm. Finally, the model determines whether the spectra have been measured out to the baseline (e,f) and use a different fitting procedure in each of these cases (g,h). The model then outputs a 2D distribution of the AuNRs fitted to the sample (i). Rational for selecting the 795 nm cutoff is shown in (j) and the validity of the differing methods for the measured baseline and the discarding of uncertain spectra are shown in (k,l). The overlap metric used in (j–l) is the overlap of the predicted AuNR population and the measured AuNR population using TEM, and a full description of this metric can be found in Figure S1. A detailed description of the full model workflow can be found in the Supporting Information, section "Spectral Morphology Analysis Details".

METHODS

Materials. Hexadecyltrimethylammonium bromide (CTAB, 98.0%) was purchased from TCI America. Hydrogen tetrachloroaurate trihydrate ($HAuCl_4 \cdot 3H_2O$, 99.9%), silver nitrate ($AgNO_3$, 99.0%), and sodium borohydride ($NaBH_4$, 99.99%) were obtained from Sigma-Aldrich. Diglycol methyl ether (diglyme 99.5%) was used to dissolve $NaBH_4$ and was purchased from Sigma-Aldrich. Hydroquinone (99%) was purchased from Sigma-Aldrich. $NaBH_4$ powder was stored in a nitrogen glovebox. $HAuCl_4 \cdot 3H_2O$, hydroquinone, and $AgNO_3$ were stored in a vacuum desiccator at room temperature. Deionized water was used for all aqueous solutions. All chemicals were used without further purification.

Automated Size Prediction from Absorption Spectra. AuNR morphology prediction from absorption spectra of colloidal samples is based on the basic optical properties of colloidal samples of AuNRs. In short, the overall spectrum can be approximated as a sum of the absorption of each particle in the colloid, provided nothing else is absorbing or scattering in the energy range of the spectrum. It then becomes possible to determine the sizes of AuNRs present in a sample by fitting the relative contribution of AuNRs of different sizes and finding the distribution that best rebuilds the sample's spectrum. These assumptions serve as the basis of our SMA.

The basis set for spectral fitting in our model consists of numerically simulated single particle spectra of AuNRs from the scuff-em simulation procedure, which simulates absorption spectra using boundary-element methods, as shown in Figure 1a,b.[47] The accuracy of these simulations and their ability to accurately reproduce a full experimental absorption spectrum have been shown by comparison with TEM measurements (Figure S4). These single particle spectra of individual nanorods have a Lorentzian line shape, although it should be noted that the shape of the ensemble spectrum is determined by the size distribution rather than the individual line shape (Figure 1b,d). The SMA uses these single particle spectra to reproduce a colloid's absorption spectrum by generating a size distribution based on AuNR mean length/standard deviation, mean diameter/standard deviation, and the correlation between the length and diameter distributions. This distribution is then applied to the basis set, building an ensemble spectrum corresponding to the predicted size distribution, as shown in Figure 1c,d. This procedure varies the predicted AuNR size distribution and returns the values of the five parameters that build the best fit, indicating the predicted population of AuNRs in this sample as well as the χ square between the fitted and experimental spectrum as a measure of how well the fit has replicated the experimental spectrum. In cases where there are multiple stable fits, unless specified otherwise, the prediction is the fit that has the lowest χ square value between the two spectra. The accuracy of this model at predicting size distributions across a broad range of size parameters has been validated by manual TEM analysis by our group and extracted spectra from literature results on AuNR synthesis.[40,48−67] The model imposes certain physical assumptions on the population distribution to prevent theoretically possible but physically highly unlikely populations from being returned as the best fit. These assumptions are

https://doi.org/10.1021/acsnano.4c09753
ACS Nano 2024, 18, 34646−34655

1. there is some degree of correlation between the lengths and diameters in the 2D population distribution, and the degree of correlation is fit as a part of the fitting process,
2. the population distribution is normally distributed for both lengths and diameters, and
3. the standard deviation is capped to prevent nonphysical parameters, for example, standard deviations so large the tails extend into regions where there are no simulated spectra.

To account for situations where there has been low shape yield and/or not fully cleaned samples, resulting in unreacted growth solution still present in the colloid, the spectrum is fit from 795 nm onward, rather than using the full spectrum. This allows the model to be applicable to colloids producing low shape yield of AuNRs as it removes the degeneracy around the transverse peak, where intensity originates from undesirable AuNS and the transverse mode of AuNRs. 795 nm was selected as the cutoff by determining the location where our training data maximized accuracy and number of spectra fit by the procedure, which are roughly inversely proportional. This is shown in Figure 4j, and a more detailed description of these steps and their justification is found in the Supporting Information, section "Spectral Morphology Analysis Details".

Automated Size Prediction Model Validation. The accuracy of our size prediction model was validated using samples generated from a high-throughput AuNR synthesis run and spectra extracted from the literature. Our validation high-throughput synthesis procedure produced 20 samples deemed suitable for validation. This required at least moderate shape purity as many reaction conditions in our high-throughput experiment produced a significant number of AuNS. The criteria for moderate shape purity was that the ratio between the transverse plasmon peak at roughly 520 nm, where AuNS absorption occurs, and the longitudinal peak intensity had to be less than one. Additionally, only samples following the filtering criteria set out in Figure 4 were fit. All of the validation high-throughput samples fitting the selection criteria were fit successfully. At least 500 particles were measured for each high-throughput synthesis sample by taking between 50 and 100 TEM images. The particles were then measured using AutoDetect-mNP, an automated size and shape detection algorithm for TEM images of metal nanoparticles.[20]

In the case of the literature spectra, 86 spectra were extracted with reported size information. Of these, 19 were discarded due to either highly irregular synthesis conditions deemed likely to impact the spectra (i.e., large volumes of biological additives) or noted systematic errors in spectral processing (spectra that did not baseline subtract the H_2O peak in the NIR, etc.). 12 were discarded due to the spectra being incomplete, determined by the longitudinal peak ending before the fwhm of the peak. 10 were discarded due to the reported size parameters being outside the range of the lower bound of our diameters, denoted by a threshold set 1 nm higher than our lowest diameter value, 5 nm. This threshold was chosen due to observations that fitted populations with the mean diameter lower than 6 nm often had appreciable density in regions where there were no simulated spectra. Four additional spectra were discarded due to their longitudinal peak being too high in energy (see Figure 4c,d). 17 were returned as too uncertain to be fit (see Figure 4g), and an additional 3 failed due to the values hitting the bounds of the prediction space. This resulted in 21 literature spectra that were added to our validation set of labeled spectra. The full validation set contained 41 labeled spectra, which are listed in Figure 2.

Manual AuNR Synthesis. AuNRs were prepared using a modified version of the procedure described by Vigderman and Zubarev.[33] In a general synthesis, aqueous solutions of CTAB, $HAuCl_4$, and $AgNO_3$, in that order, were added to a 1 mL glass vial with a stir bar. Then, an aqueous solution of hydroquinone was added to the reaction mixture to reduce Au(III) to Au(I), inducing a color change from yellow to clear. After waiting 10 min, a solution of $NaBH_4$ dissolved in diglyme and sonicated for 10 min was added to the solution under rapid stirring to induce the formation of AuNRs. Stirring was then stopped after half an hour, and the solutions were allowed to grow overnight to ensure that the reaction had completed. Then, each solution was centrifuged at 10,000 rpm for 30 min and resuspended in DI water under gentle sonication to disperse the pellet.

Absorbance Spectroscopy. UV−vis absorption spectroscopy of the synthesized AuNRs was conducted using a Shimadzu UV-3600 double beam spectrometer. Samples were prepared by resuspending the centrifuged sample in 1 mL of DI water and then diluting 300 μL of this sample with 2.7 mL of DI water. Before measurements, a background spectrum was recorded and subtracted by using a cuvette filled with 3 mL of DI water.

Transmission Electron Microscopy. Images of the AuNR samples were taken with an FEI Tecnai T20 transmission electron microscope equipped with a Gatan RIO16IS camera and a LaB_6 filament. All images were recorded under 200 kV accelerating voltage. Samples were prepared for TEM by drop casting from the 3 mL sample used for absorption spectral analysis, which was found to have the appropriate concentration, onto a carbon support with 400 copper mesh. Samples were dried overnight by placing them under vacuum.

High-Throughput Synthesis. High-throughput synthesis of AuNRs was performed by using a Hamilton Microlab NIMBUS4 liquid handling robot. For high-throughput synthesis, fresh aqueous solutions of CTAB (100 mM), hydroquinone (60 mM), $HAuCl_4$ (4 mM), $AgNO_3$ (5 mM), and $NaBH_4$ (0.3 mM) were prepared for each run. These solutions were then added to single use 1 mL glass vials in the order DI H_2O, CTAB, $HAuCl_4$, $AgNO_3$, hydroquinone, and $NaBH_4$ while the entire plate was heated to 30 °C and shaken at 300 rpm. Shaking continued for half an hour after the final addition was completed, and the plate was then left undisturbed for 4 h. The samples were then removed from the plate and placed in a dark cabinet and wrapped in aluminum foil to continue reacting overnight.

Several components of the typical hydroquinone seedless synthesis procedure[33] were changed to produce a reaction that was compatible with our liquid handling synthesis robot setup. The overall scale of the reaction was significantly decreased to ensure that a 96-well plate could be used for high-throughput synthesis, optimizing the number of reactions achieved with each run. This necessitated the use of 1 mL vials, producing 0.5 mL of sample, which is roughly a factor of 20 below the volume produced by the previously reported procedures. Additionally, to maximize the liquid handling precision of the NIMBUS robot, the minimum volumes for each reagent are maintained at 5 μL, necessitating a lower concentration of stock solutions such as $NaBH_4$. Diglyme was chosen as a polar, aprotic solvent to eliminate background reactions of $NaBH_4$ with H_2O. This work found $NaBH_4$ to be stable in diglyme for over 24 h (Figure S5). The enhanced stability also allows for more flexibility with the reaction procedure, allowing reactions to be performed with multiple additions of $NaBH_4$ and potentially allowing options for more advanced procedures, such as AuNR synthesis with a syringe pump. Finally, the stability of the stock solution allows for improved reproducibility of the synthesis procedure, potentially overcoming a chronic problem in the field (Figures S5 and S6).

ASSOCIATED CONTENT

Data Availability Statement

The data set of simulated AuNR spectra, the high-throughput synthesis reaction conditions, resulting spectra, size predictions, and TEM images used for analysis, literature spectra, size predictions, true sizes, and reaction conditions (when applicable) and the code generating the size prediction model can be found at https://github.com/smglsn12/AuNR-SMA.

Supporting Information

The Supporting Information is available free of charge at https://pubs.acs.org/doi/10.1021/acsnano.4c09753.

Additional information on the size prediction model, high-throughput synthesis procedure, ML model con-

https://doi.org/10.1021/acsnano.4c09753
ACS Nano 2024, 18, 34646−34655

struction, data collection and processing procedures, and further discussion (PDF)

AUTHOR INFORMATION

Corresponding Authors

Samuel P. Gleason − *Department of Chemistry, University of California Berkeley, Berkeley, California 94720, United States; Materials Sciences Division, Lawrence Berkeley National Laboratory, Berkeley, California 94720, United States;* orcid.org/0000-0002-1787-6266; Email: smglsn12@berkeley.edu

A. Paul Alivisatos − *Department of Chemistry, University of California Berkeley, Berkeley, California 94720, United States; Department of Materials Science and Engineering, University of California, Berkeley, Berkeley, California 94720, United States; Materials Sciences Division, Lawrence Berkeley National Laboratory, Berkeley, California 94720, United States; Kavli Energy NanoScience Institute, Berkeley, California 94720, United States;* Present Address: Department of Chemistry, University of Chicago, Chicago, Illinois 60637, United States; orcid.org/0000-0001-6895-9048; Email: paul.alivisatos@uchicago.edu

Authors

Jakob C. Dahl − *Department of Chemistry, University of California Berkeley, Berkeley, California 94720, United States; Materials Sciences Division, Lawrence Berkeley National Laboratory, Berkeley, California 94720, United States; Molecular Foundry, Lawrence Berkeley National Laboratory, Berkeley, California 94720, United States;* orcid.org/0000-0002-1443-8877

Mahmoud Elzouka − *Lawrence Berkeley National Laboratory, Berkeley, California 94720, United States*

Xingzhi Wang − *Department of Chemistry, University of California Berkeley, Berkeley, California 94720, United States; Materials Sciences Division, Lawrence Berkeley National Laboratory, Berkeley, California 94720, United States*

Dana O. Byrne − *Department of Chemistry, University of California Berkeley, Berkeley, California 94720, United States; Materials Sciences Division, Lawrence Berkeley National Laboratory, Berkeley, California 94720, United States*

Hannah Cho − *Department of Chemistry, University of California Berkeley, Berkeley, California 94720, United States*

Mumtaz Gababa − *Department of Chemistry, University of California Berkeley, Berkeley, California 94720, United States*

Ravi S. Prasher − *Lawrence Berkeley National Laboratory, Berkeley, California 94720, United States;* orcid.org/0000-0002-3282-7147

Sean Lubner − *Lawrence Berkeley National Laboratory, Berkeley, California 94720, United States*

Emory M. Chan − *Molecular Foundry, Lawrence Berkeley National Laboratory, Berkeley, California 94720, United States;* orcid.org/0000-0002-5655-0146

Complete contact information is available at: https://pubs.acs.org/10.1021/acsnano.4c09753

Author Contributions

S.P.G. developed, validated, and applied the automated size prediction model, developed the high-throughput synthesis procedure, conducted the high-throughput experiments, and wrote the manuscript. J.C.D. provided training, expertise, and conducted high-throughput synthesis experiments, provided advising on the automated size prediction model construction, and developed the machine learning models discussed in Application 2. M.E. generated the simulated AuNR spectra. X.W. provided automated size prediction modeling for the TEM images taken in this work. D.O.B. took the validation TEM images necessary to validate the size prediction model. M.G. and H.C. extracted and labeled literature spectra. R.P. and S.L. provided advising and expertise related to the simulated AuNR spectra generation. E.C. provided advising, expertise, and training for the high-throughput AuNR synthesis experiments. A.P.A. provided experimental AuNR synthesis knowledge, project planning, led the collaboration, and designed the scope of this work. All authors read, edited, and approved the final manuscript.

Notes

The authors declare no competing financial interest.

ACKNOWLEDGMENTS

Work at the Molecular Foundry was supported by the Office of Science, Office of Basic Energy Sciences, of the U.S. Department of Energy under Contract no. DE-AC02-05CH11231. Other work reported here was supported by the U.S. Department of Energy, Office of Science, Office of Basic Energy Sciences, Materials Sciences and Engineering Division, under Contract no. DE-AC02-05-CH11231 within the Data Science for Data-Driven Synthesis Science grant (KCD2S2). Computational resources for simulations of AuNR spectra were provided by the Lawrencium computational cluster resource provided by the IT Division at the Lawrence Berkeley National Laboratory with funding by the Director, Office of Science, Office of Basic Energy Sciences, of the U.S. Department of Energy under Contract no. DE-AC02-05CH11231. J.C.D. acknowledges funding through the NSF-GRFP program under DGE 1752814 and the Kavli Nano-Science Institute, University of California, Berkeley through the Philomathia Graduate Student Fellowship.

REFERENCES

(1) Tong, L.; Wei, Q.; Wei, A.; Cheng, J.-X. Gold nanorods as contrast agents for biological imaging: optical properties, surface conjugation and photothermal effects. *Photochem. Photobiol.* **2009**, *85*, 21−32.

(2) Jain, P. K.; Huang, X.; El-Sayed, I. H.; El-Sayed, M. A. Noble Metals on the Nanoscale: Optical and Photothermal Properties and Some Applications in Imaging, Sensing, Biology, and Medicine. *Acc. Chem. Res.* **2008**, *41*, 1578−1586.

(3) Kang, X.; Guo, X.; Niu, X.; An, W.; Li, S.; Liu, Z.; Yang, Y.; Wang, N.; Jiang, Q.; Yan, C.; Wang, H.; Zhang, Q. Photothermal therapeutic application of gold nanorods-porphyrin-trastuzumab complexes in HER2-positive breast cancer. *Sci. Rep.* **2017**, *7*, 42069.

(4) Mallick, S.; Sun, I.-C.; Kim, K.; Yi, D. K. Silica coated gold nanorods for imaging and photo-thermal therapy of cancer cells. *J. Nanosci. Nanotechnol.* **2013**, *13*, 3223−3229.

(5) Choi, W. I.; Sahu, A.; Kim, Y. H.; Tae, G. Photothermal cancer therapy and imaging based on gold nanorods. *Ann. Biomed. Eng.* **2012**, *40*, 534−546.

(6) Mbalaha, Z. S.; Edwards, P. R.; Birch, D. J.; Chen, Y. Synthesis of Small Gold Nanorods and Their Subsequent Functionalization with Hairpin Single Stranded DNA. *ACS Omega* **2019**, *4*, 13740−13746.
(7) Sebastián, V.; Lee, S.-K.; Zhou, C.; Kraus, M. F.; Fujimoto, J. G.; Jensen, K. F. One-step continuous synthesis of biocompatible gold nanorods for optical coherence tomography. *Chem. Commun.* **2012**, *48*, 6654−6656.
(8) Zhu, J.; Yong, K.-T.; Roy, I.; Hu, R.; Ding, H.; Zhao, L.; Swihart, M. T.; He, G. S.; Cui, Y.; Prasad, P. N. Additive controlled synthesis of gold nanorods (GNRs) for two-photon luminescence imaging of cancer cells. *Nanotechnology* **2010**, *21*, 285106.
(9) Amendola, V.; Pilot, R.; Frasconi, M.; Maragò, O. M.; Iatì, M. A. Surface plasmon resonance in gold nanoparticles: a review. *J. Phys.: Condens. Matter* **2017**, *29*, 203002.
(10) Ou, Y.; Wang, X.; Lai, K.; Huang, Y.; Rasco, B. A.; Fan, Y. Gold Nanorods as Surface-Enhanced Raman Spectroscopy Substrates for Rapid and Sensitive Analysis of Allura Red and Sunset Yellow in Beverages. *J. Agric. Food Chem.* **2018**, *66*, 2954−2961.
(11) de Barros, A.; Shimizu, F. M.; de Oliveira, C. S.; Sigoli, F. A.; dos Santos, D. P.; Mazali, I. O. Dynamic Behavior of Surface-Enhanced Raman Spectra for Rhodamine 6G Interacting with Gold Nanorods: Implication for Analyses under Wet versus Dry Conditions. *ACS Appl. Nano Mater.* **2020**, *3*, 8138−8147.
(12) Alvarez-Puebla, R. A.; Agarwal, A.; Manna, P.; Khanal, B. P.; Aldeanueva-Potel, P.; Carbó-Argibay, E.; Pazos-Pérez, N.; Vigderman, L.; Zubarev, E. R.; Kotov, N. A.; et al. Gold nanorods 3D-supercrystals as surface enhanced Raman scattering spectroscopy substrates for the rapid detection of scrambled prions. *Proc. Natl. Acad. Sci. U.S.A.* **2011**, *108*, 8157−8161.
(13) Karg, M.; König, T. A.; Retsch, M.; Stelling, C.; Reichstein, P. M.; Honold, T.; Thelakkat, M.; Fery, A. Colloidal self-assembly concepts for light management in photovoltaics. *Mater. Today* **2015**, *18*, 185−205.
(14) Mubeen, S.; Lee, J.; Lee, W. r.; Singh, N.; Stucky, G. D.; Moskovits, M. On the Plasmonic Photovoltaic. *ACS Nano* **2014**, *8*, 6066−6073.
(15) Link, S.; Mohamed, M. B.; El-Sayed, M. A. Simulation of the Optical Absorption Spectra of Gold Nanorods as a Function of Their Aspect Ratio and the Effect of the Medium Dielectric Constant. *J. Phys. Chem. B* **1999**, *103*, 3073−3077.
(16) Eustis, S.; El-Sayed, M. Aspect Ratio Dependence of the Enhanced Flourescense Intensity of Gold Nanorods: Experimental and Simulation Study. *J. Phys. Chem. B* **2005**, *109*, 16350−16356.
(17) Ringe, E.; Langille, M. R.; Sohn, K.; Zhang, J.; Huang, J.; Mirkin, C. A.; Van Duyne, R. P.; Marks, L. D. Plasmon Length: A Universal Parameter to Describe Size Effects in Gold Nanoparticles. *J. Phys. Chem. Lett.* **2012**, *3*, 1479−1483.
(18) Burrows, N. D.; Harvey, S.; Idesis, F. A.; Murphy, C. J. Understanding the Seed-Mediated Growth of Gold Nanorods through a Fractional Factorial Design of Experiments. *Langmuir* **2017**, *33*, 1891−1907.
(19) Lee, B.; Yoon, S.; Lee, J. W.; Kim, Y.; Chang, J.; Yun, J.; Ro, J. C.; Lee, J.-S.; Lee, J. H. Statistical Characterization of the Morphologies of Nanoparticles through Machine Learning Based Electron Microscopy Image Analysis. *ACS Nano* **2020**, *14*, 17125−17133.
(20) Wang, X.; Li, J.; Ha, H. D.; Dahl, J. C.; Ondry, J. C.; Moreno-Hernandez, I.; Head-Gordon, T.; Alivisatos, A. P. AutoDetect-mNP: An Unsupervised Machine Learning Algorithm for Automated Analysis of Transmission Electron Microscope Images of Metal Nanoparticles. *JACS Au* **2021**, *1*, 316−327.
(21) Dahl, J. C.; Wang, X.; Huang, X.; Chan, E. M.; Alivisatos, A. P. Elucidating the Weakly Reversible Cs−Pb−Br Perovskite Nanocrystal Reaction Network with High-Throughput Maps and Transformations. *J. Am. Chem. Soc.* **2020**, *142*, 11915−11926.
(22) Laramy, C. R.; Brown, K. A.; O'Brien, M. N.; Mirkin, C. A. High-Throughput, Algorithmic Determination of Nanoparticle Structure from Electron Microscopy Images. *ACS Nano* **2015**, *9*, 12488−12495.
(23) Mulligan, S. K.; Speir, J. A.; Razinkov, I.; Cheng, A.; Crum, J.; Jain, T.; Duggan, E.; Liu, E.; Nolan, J. P.; Carragher, B.; Potter, C. S. Multiplexed TEM Specimen Preparation and Analysis of Plasmonic Nanoparticles. *Microsc. Microanal.* **2015**, *21*, 1017−1025.
(24) Shiratori, K.; Bishop, L. D. C.; Ostovar, B.; Baiyasi, R.; Cai, Y.-Y.; Rossky, P. J.; Landes, C. F.; Link, S. Machine-Learned Decision Trees for Predicting Gold Nanorod Sizes from Spectra. *J. Phys. Chem. C* **2021**, *125*, 19353−19361.
(25) Pashkov, D. M.; Guda, A. A.; Kirichkov, M. V.; Guda, S. A.; Martini, A.; Soldatov, S. A.; Soldatov, A. V. Quantitative Analysis of the UV−Vis Spectra for Gold Nanoparticles Powered by Supervised Machine Learning. *J. Phys. Chem. C* **2021**, *125*, 8656−8666.
(26) Slaughter, L. S.; Chang, W.-S.; Swanglap, P.; Tcherniak, A.; Khanal, B. P.; Zubarev, E. R.; Link, S. Single-Particle Spectroscopy of Gold Nanorods beyond the Quasi-Static Limit: Varying the Width at Constant Aspect Ratio. *J. Phys. Chem. C* **2010**, *114*, 4934−4938.
(27) Encina, E. R.; Coronado, E. A. Resonance Conditions for Multipole Plasmon Excitations in Noble Metal Nanorods. *J. Phys. Chem. C* **2007**, *111*, 16796−16801.
(28) Salley, D.; Keenan, G.; Grizou, J.; Sharma, A.; Martín, S.; Cronin, L. A nanomaterials discovery robot for the Darwinian evolution of shape programmable gold nanoparticles. *Nat. Commun.* **2020**, *11*, 2771.
(29) Jiang, Y.; Salley, D.; Sharma, A.; Keenan, G.; Mullin, M.; Cronin, L. An artificial intelligence enabled chemical synthesis robot for exploration and optimization of nanomaterials. *Sci. Adv.* **2022**, *8*, No. eabo2626.
(30) Vaddi, K.; Chiang, H. T.; Pozzo, L. D. Autonomous retrosynthesis of gold nanoparticles via spectral shape matching. *Digital Discovery* **2022**, *1*, 502−510.
(31) Yazdani, S.; Daneshkhah, A.; Diwate, A.; Patel, H.; Smith, J.; Reul, O.; Cheng, R.; Izadian, A.; Hajrasouliha, A. R. Model for Gold Nanoparticle Synthesis: Effect of pH and Reaction Time. *ACS Omega* **2021**, *6*, 16847−16853.
(32) Jana, N. R. Gram-scale synthesis of soluble, near-monodisperse gold nanorods and other anisotropic nanoparticles. *Small* **2005**, *1*, 875−882.
(33) Vigderman, L.; Zubarev, E. R. High-Yield Synthesis of Gold Nanorods with Longitudinal SPR Peak Greater than 1200 nm Using Hydroquinone as a Reducing Agent. *Chem. Mater.* **2013**, *25*, 1450−1457.
(34) Mulekar, M. S.; Mishra, S. N. Overlap Coefficients of Two Normal Densities: Equal Means Case. *J. Jpn. Stat. Soc.* **1994**, *24*, 169−180.
(35) Liu, K.; Bu, Y.; Zheng, Y.; Jiang, X.; Yu, A.; Wang, H. Seedless Synthesis of Monodispersed Gold Nanorods with Remarkably High Yield: Synergistic Effect of Template Modification and Growth Kinetics Regulation. *Chem.—Eur. J.* **2017**, *23*, 3291−3299.
(36) Nikoobakht, B.; El-Sayed, M. A. Preparation and Growth Mechanism of Gold Nanorods (NRs) Using Seed-Mediated Growth Method. *Chem. Mater.* **2003**, *15*, 1957−1962.
(37) Jackson, S. R.; McBride, J. R.; Rosenthal, S. J.; Wright, D. W. Where's the Silver? Imaging Trace Silver Coverage on the Surface of Gold Nanorods. *J. Am. Chem. Soc.* **2014**, *136*, 5261−5263.
(38) Pedregosa, F.; et al. Scikit-learn: Machine Learning in Python. *J. Mach. Learn. Res.* **2011**, *12*, 2825−2830.
(39) Dahl, J. C.; Niblett, S.; Cho, Y.; Wang, X.; Zhang, Y.; Chan, E. M.; Alivisatos, A. P. Scientific Machine Learning of 2D Perovskite Nanosheet Formation. *J. Am. Chem. Soc.* **2023**, *145*, 23076−23087.
(40) Zhang, L.; Xia, K.; Lu, Z.; Li, G.; Chen, J.; Deng, Y.; Li, S.; Zhou, F.; He, N. Efficient and Facile Synthesis of Gold Nanorods with Finely Tunable Plasmonic Peaks from Visible to Near-IR Range. *Chem. Mater.* **2014**, *26*, 1794−1798.
(41) Wang, W.; Li, J.; Lan, S.; Rong, L.; Liu, Y.; Sheng, Y.; Zhang, H.; Yang, B. Seedless synthesis of gold nanorods using resveratrol as a reductant. *Nanotechnology* **2016**, *27*, 165601.
(42) Park, J.-E.; Lee, Y.; Nam, J.-M. Precisely Shaped, Uniformly Formed Gold Nanocubes with Ultrahigh Reproducibility in Single-

https://doi.org/10.1021/acsnano.4c09753
ACS Nano 2024, 18, 34646−34655

Particle Scattering and Surface-Enhanced Raman Scattering. *Nano Lett.* **2018**, *18*, 6475−6482.
(43) Scarabelli, L.; Coronado-Puchau, M.; Giner-Casares, J. J.; Langer, J.; Liz-Marzán, L. M. Monodisperse Gold Nanotriangles: Size Control, Large-Scale Self-Assembly, and Performance in Surface-Enhanced Raman Scattering. *ACS Nano* **2014**, *8*, 5833−5842.
(44) Rekha, C.; Nayar, V.; Gopchandran, K. Synthesis of highly stable silver nanorods and their application as SERS substrates. *J. Sci.:Adv. Mater. Devices* **2018**, *3*, 196−205.
(45) Ten, A.; West, C. A.; Jeong, S.; Hopper, E. R.; Wang, Y.; Zhu, B.; Ramasse, Q. M.; Ye, X.; Ringe, E. Bimetallic copper palladium nanorods: plasmonic properties and palladium content effects. *Nanoscale Adv.* **2023**, *5*, 6524−6532.
(46) Aubert, T.; Golovatenko, A. A.; Samoli, M.; Lermusiaux, L.; Zinn, T.; Abécassis, B.; Rodina, A. V.; Hens, Z. General Expression for the Size-Dependent Optical Properties of Quantum Dots. *Nano Lett.* **2022**, *22*, 1778−1785.
(47) Elzouka, M.; Yang, C.; Albert, A.; Prasher, R. S.; Lubner, S. D. Interpretable Forward and Inverse Design of Particle Spectral Emissivity Using Common Machine-Learning Models. *Cell Rep. Phys. Sci.* **2020**, *1*, 100259.
(48) Requejo, K. I.; Liopo, A. V.; Derry, P. J.; Zubarev, E. R. Accelerating Gold Nanorod Synthesis with Nanomolar Concentrations of Poly(vinylpyrrolidone). *Langmuir* **2017**, *33*, 12681−12688.
(49) Zhang, Q.; Han, L.; Jing, H.; Blom, D. A.; Lin, Y.; Xin, H. L.; Wang, H. Facet Control of Gold Nanorods. *ACS Nano* **2016**, *10*, 2960−2974.
(50) Scarabelli, L.; Grzelczak, M.; Liz-Marzán, L. M. Tuning Gold Nanorod Synthesis through Prereduction with Salicylic Acid. *Chem. Mater.* **2013**, *25*, 4232−4238.
(51) del Caño, R.; Gisbert-González, J. M.; González-Rodríguez, J.; Sánchez-Obrero, G.; Madueño, R.; Blázquez, M.; Pineda, T. Effective replacement of cetyltrimethylammonium bromide (CTAB) by mercaptoalkanoic acids on gold nanorod (AuNR) surfaces in aqueous solutions. *Nanoscale* **2020**, *12*, 658−668.
(52) Requejo, K. I.; Liopo, A. V.; Zubarev, E. R. Synthesis of Gold Nanorods Using Poly(vinylpyrrolidone) of Different Molecular Weights as an Additive. *Chem. Eur.* **2018**, *3*, 12192−12197.
(53) Requejo, K. I.; Liopo, A. V.; Zubarev, E. R. Gold Nanorod Synthesis with Small Thiolated Molecules. *Langmuir* **2020**, *36*, 3758−3769.
(54) Wei, M.-Z.; Deng, T.-S.; Zhang, Q.; Cheng, Z.; Li, S. Seed-Mediated Synthesis of Gold Nanorods at Low Concentrations of CTAB. *ACS Omega* **2021**, *6*, 9188−9195.
(55) Lai, J.; Zhang, L.; Niu, W.; Qi, W.; Zhao, J.; Liu, Z.; Zhang, W.; Xu, G. One-pot synthesis of gold nanorods using binary surfactant systems with improved monodispersity, dimensional tunability and plasmon resonance scattering properties. *Nanotechnology* **2014**, *25*, 125601.
(56) Ye, X.; Zheng, C.; Chen, J.; Gao, Y.; Murray, C. B. Using Binary Surfactant Mixtures To Simultaneously Improve the Dimensional Tunability and Monodispersity in the Seeded Growth of Gold Nanorods. *Nano Lett.* **2013**, *13*, 765−771.
(57) Gallagher, R.; Zhang, X.; Altomare, A.; Lawrence, D., Jr.; Shawver, N.; Tran, N.; Beazley, M.; Chen, G. pH-mediated synthesis of monodisperse gold nanorods with quantitative yield and molecular level insight. *Nano Res.* **2021**, *14*, 1167−1174.
(58) Link, S.; El-Sayed, M. A. Spectral Properties and Relaxation Dynamics of Surface Plasmon Electronic Oscillations in Gold and Silver Nanodots and Nanorods. *J. Phys. Chem. B* **1999**, *103*, 8410−8426.
(59) Xu, X.; Zhao, Y.; Xue, X.; Huo, S.; Chen, F.; Zou, G.; Liang, X.-J. Seedless synthesis of high aspect ratio gold nanorods with high yield. *J. Mater. Chem. A* **2014**, *2*, 3528−3535.
(60) Salavatov, N. A.; Dement'eva, O. V.; Mikhailichenko, A. I.; Rudoy, V. M. Some Aspects of Seedless Synthesis of Gold Nanorods. *Colloid J.* **2018**, *80*, 541−549.
(61) Ye, X.; Jin, L.; Caglayan, H.; Chen, J.; Xing, G.; Zheng, C.; Doan-Nguyen, V.; Kang, Y.; Engheta, N.; Kagan, C. R.; Murray, C. B. Improved Size-Tunable Synthesis of Monodisperse Gold Nanorods through the Use of Aromatic Additives. *ACS Nano* **2012**, *6*, 2804−2817.
(62) Ye, X.; Gao, Y.; Chen, J.; Reifsnyder, D. C.; Zheng, C.; Murray, C. B. Seeded Growth of Monodisperse Gold Nanorods Using Bromide-Free Surfactant Mixtures. *Nano Lett.* **2013**, *13*, 2163−2171.
(63) Roach, L.; Ye, S.; Moorcroft, S. C. T.; Critchley, K.; Coletta, P. L.; Evans, S. D. Morphological control of seedlessly-synthesized gold nanorods using binary surfactants. *Nanotechnology* **2018**, *29*, 135601.
(64) Huang, H.; Li, H.; Wang, H.; Li, J.; Li, P.; Chen, Q.; Chen, Y.; Chu, P. K.; Li, B.; Yu, X.-F. Morphological control of gold nanorods via thermally driven bi-surfactant growth and application for detection of heavy metal ions. *Nanotechnology* **2018**, *29*, 334001.
(65) Tong, W.; Walsh, M. J.; Mulvaney, P.; Etheridge, J.; Funston, A. M. Control of Symmetry Breaking Size and Aspect Ratio in Gold Nanorods: Underlying Role of Silver Nitrate. *J. Phys. Chem. C* **2017**, *121*, 3549−3559.
(66) Liopo, A.; Wang, S.; Derry, P. J.; Oraevsky, A. A.; Zubarev, E. R. Seedless synthesis of gold nanorods using dopamine as a reducing agent. *RSC Adv.* **2015**, *5*, 91587−91593.
(67) Li, M.; Zhou, R.; Liu, X.; Tao, Q. Seedless synthesis of gold nanorods by using hydrogen peroxide as a weak reducing agent. *Spectrosc. Lett.* **2019**, *52*, 239−245.

https://doi.org/10.1021/acsnano.4c09753
ACS Nano 2024, 18, 34646−34655